



# Chemogenetic Control of Nanobodies

Helen Farrants<sup>1,2</sup>, Miroslaw Tarnawski<sup>3</sup>, Thorsten G. Müller<sup>4</sup>, Shotaro Otsuka<sup>5,6</sup>, Julien Hiblot<sup>1</sup>, Birgit Koch<sup>1</sup>, Moritz Kueblbeck<sup>5</sup>, Hans-Georg Kräusslich<sup>4</sup>, Jan Ellenberg<sup>5</sup> and Kai Johnsson<sup>1,2</sup>

**We introduce an engineered nanobody whose affinity to green fluorescent protein (GFP) can be switched on and off with small molecules. By controlling the cellular localization of GFP fusion proteins, the engineered nanobody allows interrogation of their roles in basic biological processes, an approach that should be applicable to numerous previously described GFP fusions. We also outline how the binding affinities of other nanobodies can be controlled by small molecules.**

The variable domains of heavy chain-only antibodies<sup>1</sup>, commonly abbreviated to nanobodies, can be selected to bind to a variety of targets with high affinity and selectivity, and can be functionally expressed inside cells<sup>2,3</sup>. The range of applications of nanobodies would be greatly expanded if their binding affinity toward their target could be rapidly switched on and off with a cell-permeable and nontoxic molecule. Proteins such as kinases and Cas9 have been engineered to control their activity with small molecules<sup>4–6</sup>, but these approaches have not been applied to nanobodies. Recently, nanobody-affinities have been optogenetically controlled, either by insertion of a light-oxygen-voltage domain<sup>7</sup> or by fusion of split antibody fragments to light-inducible heterodimerization domains<sup>8</sup>. However, insertion of the light-oxygen-voltage domain results in only a modest 5.5-fold change in affinity on irradiation<sup>7</sup>, whereas the activation of the split antibody fragments is irreversible<sup>8</sup>.

Here, we introduce ligand-modulated antibody fragments (LAMAs), which combine the high selectivity and specificity of nanobodies with the fast temporal control offered through the use of small molecules. LAMAs are generated by inserting a circularly permuted bacterial dihydrofolate reductase (cpDHFR)<sup>9</sup> into nanobodies. The new termini of this cpDHFR are located in an active site loop of wild-type DHFR. Furthermore, cpDHFR is partially unfolded in the absence of its cofactor nicotinamide adenine dinucleotide phosphate (NADPH) and DHFR inhibitors such as trimethoprim (TMP)<sup>10,11</sup>. TMP is a clinically approved antibacterial drug that has excellent cell and tissue permeability and is not toxic to mammalian cells. LAMAs disrupt the binding of the nanobody to its target by exploiting the change in conformation of cpDHFR on binding of NADPH and DHFR inhibitors (Fig. 1a).

The first nanobody we subjected to this approach was the enhancer nanobody for GFP<sup>12</sup>. Specifically, we inserted cpDHFR into various sites of the enhancer nanobody and measured the binding affinities of the protein chimeras to wild-type GFP (wtGFP) in the presence and absence of the ligands NADPH and TMP (Fig. 1b and Supplementary Fig. 1). The most promising insertion hits were in the complementary-determining region 3 (CDR3), which is often essential for making high affinity contacts between nanobodies and their targets<sup>13</sup>. Of these hits, we analyzed <sup>GFP</sup>LAMA<sub>F98</sub>, <sup>GFP</sup>LAMA<sub>G97</sub>

and <sup>GFP</sup>LAMA<sub>N95</sub> in greater detail (Fig. 1c–e and Supplementary Fig. 2). All three <sup>GFP</sup>LAMAs retained a single-digit nanomolar affinity to GFP in the absence of ligands. For all three nanobodies, the affinity toward GFP was dramatically decreased in the presence of NADPH and TMP such that no binding to GFP could be detected for <sup>GFP</sup>LAMA<sub>F98</sub> and <sup>GFP</sup>LAMA<sub>G97</sub> (Fig. 1c–e and Supplementary Fig. 3). For <sup>GFP</sup>LAMA<sub>F98</sub> the presence of NADPH alone also affected the binding affinity to GFP, whereas the affinity of <sup>GFP</sup>LAMA<sub>G97</sub> and <sup>GFP</sup>LAMA<sub>N95</sub> was not affected by NADPH.

The kinetics of dissociation of the complexes between GFP and <sup>GFP</sup>LAMA<sub>F98</sub> or <sup>GFP</sup>LAMA<sub>G97</sub> on addition of TMP were on the timescale of minutes:  $t_{1/2} = 34 \pm 1$  s and  $t_{1/2} = 5.6 \pm 0.5$  min for <sup>GFP</sup>LAMA<sub>F98</sub> and <sup>GFP</sup>LAMA<sub>G97</sub>, respectively (Fig. 1f,g). Subsequent removal of TMP by addition of wild-type DHFR resulted in reformation of the complexes within minutes (Fig. 1f,g). The complex could then be dissociated again by addition of an excess amount of TMP (Fig. 1f,g). The dissociation kinetics of the complexes could also be tuned using DHFR inhibitors with different affinities to DHFR (Supplementary Fig. 4). These experiments underline that <sup>GFP</sup>LAMA<sub>F98</sub> and <sup>GFP</sup>LAMA<sub>G97</sub> can be repeatedly switched on and off through the addition of DHFR inhibitors.

To understand how the cpDHFR insertion into nanobodies allowed control of binding affinities, we solved the crystal structures of <sup>GFP</sup>LAMA<sub>F98</sub> and <sup>GFP</sup>LAMA<sub>G97</sub> in complex with NADPH and TMP. No big structural changes were seen in the nanobody domain of the two LAMAs relative to enhancer nanobody. Comparing these structures with the structure of enhancer nanobody bound to GFP suggests that folded cpDHFR sterically hampers binding to GFP (Fig. 1h and Supplementary Fig. 5). The TMP-dependent control of the <sup>GFP</sup>LAMAs was abolished when GGS-linkers were inserted between cpDHFR and the nanobody (Supplementary Fig. 6), indicating that the switching of nanobody affinity did not solely arise from insertion of the protein domain.

Given the large number of nanobodies that have been selected and characterized<sup>14</sup>, we attempted to expand the LAMA concept to other targets (Supplementary Fig. 7a). Nanobodies for G-associated kinase<sup>15</sup> did not allow for cpDHFR insertion into the tried positions (Supplementary Fig. 7b,c). A nanobody for lamina-associated polypeptide 1 (ref. <sup>16</sup>) showed switching behavior on insertion of cpDHFR, with the addition of ligands increasing the affinity of the resulting LAMA (Supplementary Fig. 7d,e). A nanobody for the minimizer nanobody for GFP<sup>12</sup> showed greatly decreased affinities to its target on cpDHFR insertion, but responded to the addition of ligands (Supplementary Fig. 7f,g). A nanobody for the C-terminal region of the p24 HIV capsid protein (PDB ID 2XV6) could be readily converted into a LAMA on insertion of cpDHFR into the CDR3

<sup>1</sup>Department of Chemical Biology, Max Planck Institute for Medical Research, Heidelberg, Germany. <sup>2</sup>Institute of Chemical Sciences and Engineering, École Polytechnique Fédérale de Lausanne (EPFL), Lausanne, Switzerland. <sup>3</sup>Protein Expression and Characterization Facility, Max Planck Institute for Medical Research, Heidelberg, Germany. <sup>4</sup>Department of Infectious Diseases, Virology, University Hospital Heidelberg, Heidelberg, Germany. <sup>5</sup>Cell Biology and Biophysics Unit, European Molecular Biology Laboratory (EMBL), Heidelberg, Germany. <sup>6</sup>Present address: Max Perutz Labs, a joint venture of the University of Vienna and the Medical University of Vienna, Vienna Biocenter (VBC), Vienna, Austria. ✉e-mail: [johnsson@mr.mpg.de](mailto:johnsson@mr.mpg.de)

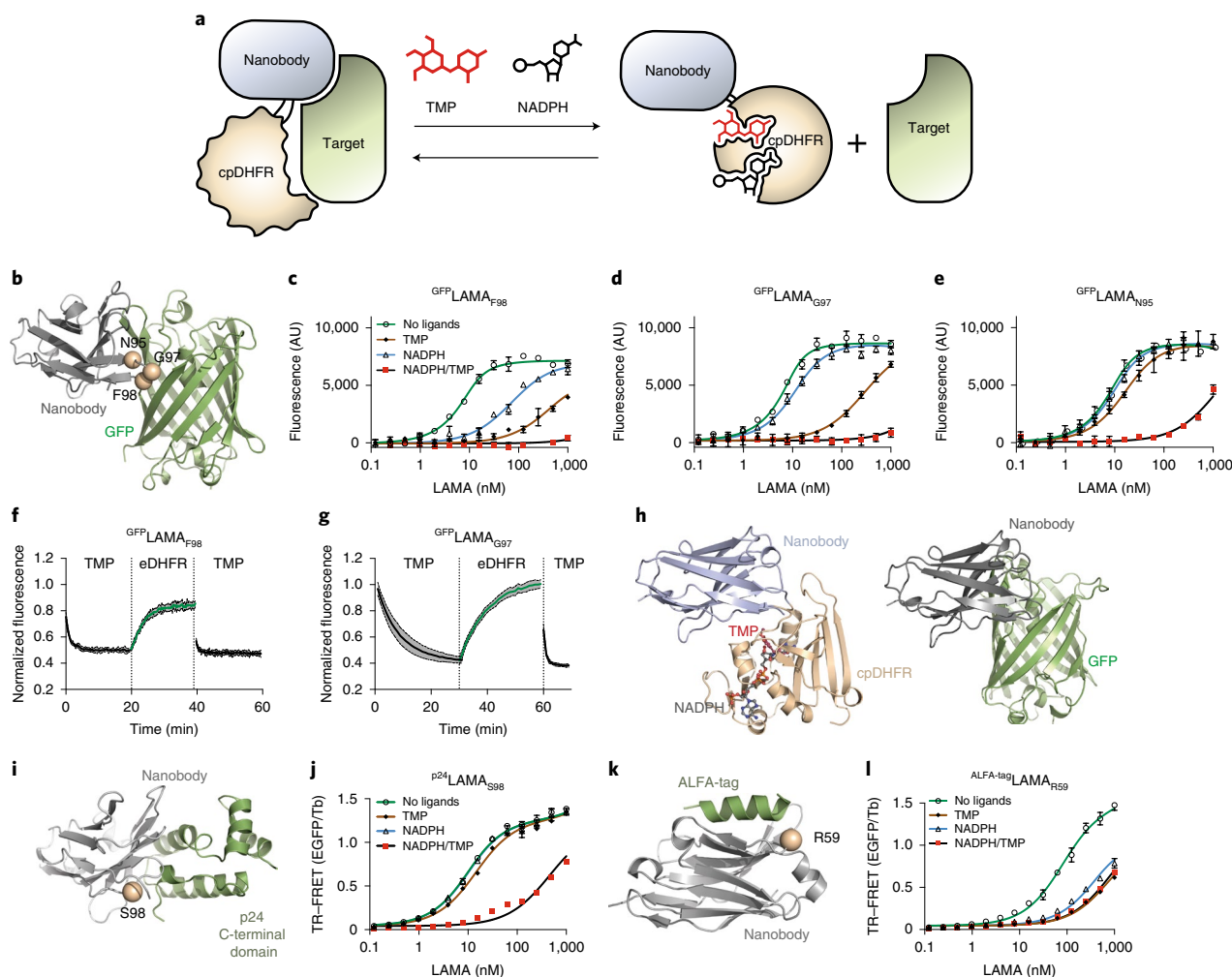


**Fig. 1 | Generation of LAMAs from nanobodies and cpDHFR.** **a**, Schematic illustration of the design principle of LAMAs. **b**, LAMA insertion positions of cpDHFR highlighted as beige spheres mapped onto the enhancer nanobody bound to GFP (PDB ID 3K1K). **c–e**, Modulation of wtGFP (10 nM) fluorescence by  $\text{GFP-LAMA}_{\text{F98}}$  (**c**),  $\text{GFP-LAMA}_{\text{G97}}$  (**d**) or  $\text{GFP-LAMA}_{\text{N95}}$  (**e**). **f, g**, Dissociation kinetics in the presence of NADPH (100  $\mu\text{M}$ ) of  $\text{GFP-LAMA}_{\text{F98}}$  (**f**) or  $\text{GFP-LAMA}_{\text{G97}}$  (**g**), from wtGFP (200 nM) on the addition of TMP (1  $\mu\text{M}$ ), followed by the competitive removal by eDHFR (8  $\mu\text{M}$ ) and addition of excess TMP (50  $\mu\text{M}$ ). **h**, Comparison of the X-ray structure of  $\text{GFP-LAMA}_{\text{F98}}$  in the presence of NADPH and TMP (PDB ID 6RUL) with the enhancer nanobody bound to GFP (PDB ID 3K1K). **i**, LAMA insertion position of cpDHFR highlighted as a beige sphere mapped onto a nanobody for p24 (PDB ID 2XV6). **j**, TR-FRET between EGFP- $\text{p}^{24}\text{LAMA}_{\text{S98}}$  and Tb-labeled SNAP-tag-p24 (5 nM). **k**, LAMA insertion position of cpDHFR highlighted as a beige sphere mapped onto a nanobody for ALFA-tag (PDB ID, 6I2G). **l**, TR-FRET of EGFP- $\text{ALFA-tag-LAMA}_{\text{R59}}$  and Tb-labeled ALFA-tag-SNAP-tag (20 nM). For all titrations, NADPH (100  $\mu\text{M}$ ), TMP (500  $\mu\text{M}$ ). All data is plotted as mean  $\pm$  s.d. For further details, see Methods.

loop (Fig. 1i and Supplementary Fig. 8). The  $\text{p}^{24}\text{LAMA}_{\text{S98}}$  showed low nanomolar affinity for p24 HIV capsid protein when no ligands were present. Neither TMP nor NADPH alone could decrease the affinity of  $\text{p}^{24}\text{LAMA}_{\text{S98}}$  for its target, but addition of both ligands reduced the affinity 70-fold (Fig. 1j). Finally, cpDHFR was inserted into several positions of NbALFA, a recently developed nanobody for the ALFA-tag<sup>17</sup>, an only 15-amino-acid-long peptide (Fig. 1k and Supplementary Fig. 9). Insertion of cpDHFR close to binding residues in CDR2 allowed switching of the affinity of the resulting  $\text{ALFA-tag-LAMA}_{\text{R59}}$  with either TMP or NADPH (Fig. 1l). These examples highlight the transferability of the LAMA approach to other nanobodies and furthermore underline that the availability of structural information on the interaction of the nanobody with its target greatly facilitates the generation of LAMAs.

The binding of both the  $\text{p}^{24}\text{LAMA}$  and  $\text{GFP-LAMAs}$  to their targets could be switched on and off through the addition of TMP in live cells (Fig. 2). Intracellular NADPH concentration in live cells is estimated to be  $3.1 \pm 0.3 \mu\text{M}$  (ref. 18). We measured the affinity of the  $\text{GFP-LAMAs}$

to NADPH to be in this range in the absence of TMP, but increase cooperatively 50-fold on the addition of TMP (Supplementary Fig. 10). The expression of the cytosolic p24 precursor polyprotein Gag in HIV transfected cells stably expressing an enhanced GFP-(EGFP)- $\text{p}^{24}\text{LAMA}_{\text{S98}}$  fusion (Fig. 2a) resulted in sequestering of the LAMA in the cytosol (Fig. 2b). However, the LAMA was released from the p24 domain of Gag by the addition of TMP within minutes, as demonstrated by diffusion of EGFP- $\text{p}^{24}\text{LAMA}_{\text{S98}}$  into the nucleus (Fig. 2b and Supplementary Fig. 11). Furthermore, fusing the  $\text{GFP-LAMAs}$  to Ntom20 (ref. 19), Lyn<sub>11</sub> (ref. 20) and a nuclear localization sequence reversibly sequestered EGFP to the outer membrane of the mitochondria, to the inner leaflet of the plasma membrane, and to the nucleus, respectively (Fig. 2c, Supplementary Fig. 12 and Supplementary Videos 1–4). The complete EGFP sequestration requires an excess of  $\text{GFP-LAMA}$  and the kinetics of the TMP-dependent release and sequestering of EGFP to the outer mitochondrial membrane occurred on a timescale of minutes, and could be repeated over several cycles (Fig. 2e,f and Supplementary Fig. 13).

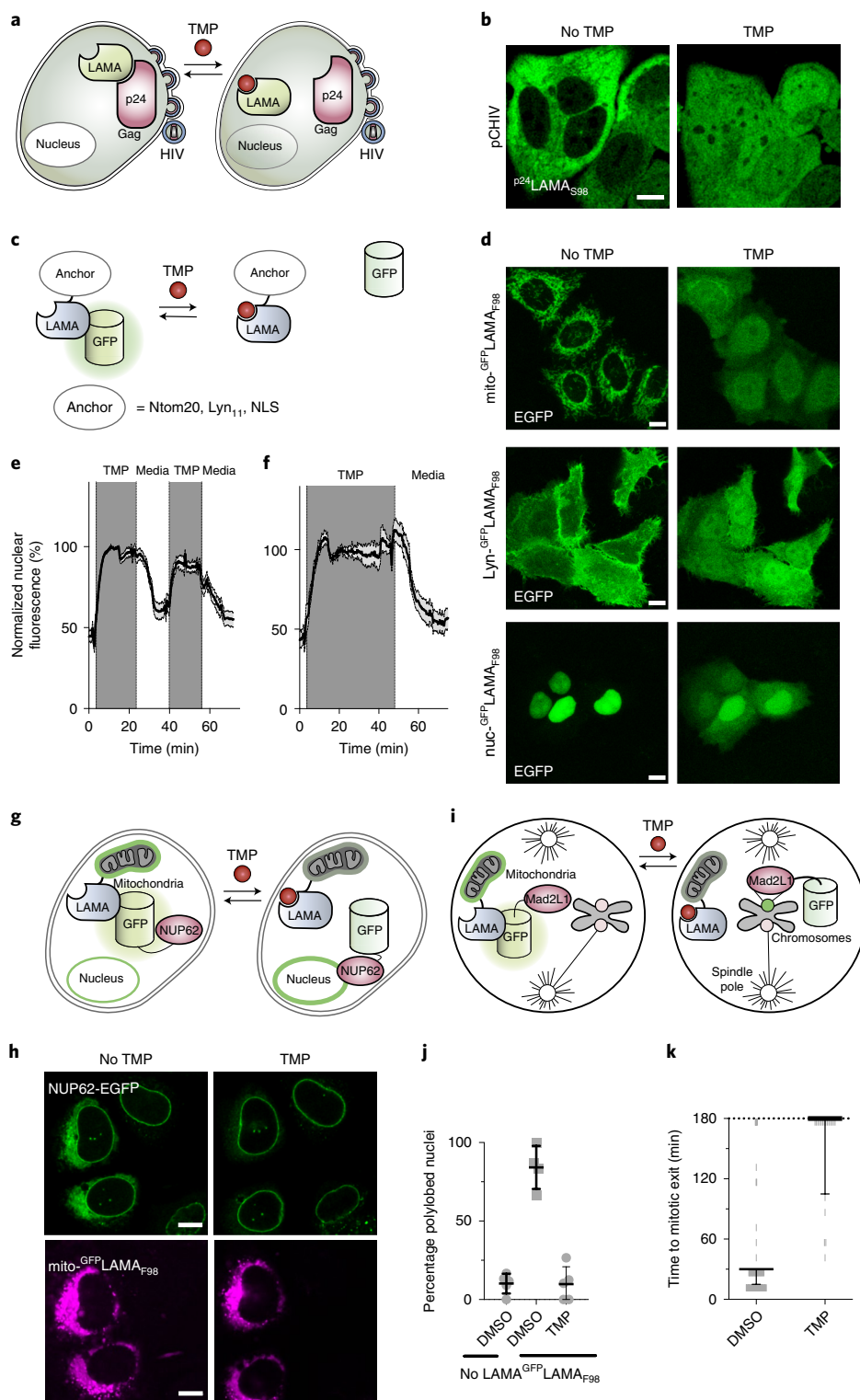


**Fig. 2 | Sequester and release of protein localization in live cells using LAMAs.** **a,b**, Schematic illustration (**a**) and live-cell imaging (**b**) of EGFP- $p24^{\text{LAMA}}_{\text{S98}}$  in cells expressing p24 as part of the Gag polyprotein after transfection with pCHIV. Images taken before and 40 min after addition of TMP. **c,d**, Schematic illustration (**c**) and live-cell imaging (**d**) of a subcellular anchored LAMA and EGFP. Images taken before and 13 min after perfusion of TMP. **e,f**, Kinetics and reversibility of EGFP sequestering to mito- $\text{GFP-LAMA}_{\text{F98}}$ . The EGFP fluorescence in the nucleus was quantified on the perfusion of TMP (dark gray area) or complete media. Mean (solid line)  $\pm$  s.e.m. (gray area) from mito- $\text{GFP-LAMA}_{\text{F98}}$  ( $N=14$  cells) (**e**) and mito- $\text{GFP-LAMA}_{\text{G97}}$  ( $N=9$  cells) (**f**). **g,h**, Schematic illustration (**g**) and live-cell imaging (**h**) of genome-edited NUP62-mEGFP and mito- $\text{GFP-LAMA}$ .  $\text{GFP-LAMA}_{\text{F98}}$  was fused to SNAP-tag and labeled with BG-TMR for visualization purposes. Cells were followed for 120 min after addition of TMP. **i**, Schematic illustration of Mad2L1-EGFP sequestered to the mitochondria by a  $\text{GFP-LAMA}$ . **j,k**, Nuclear morphology (**j**) and duration (**k**) of mitotic events during time-lapse live-cell imaging of Mad2L1-EGFP cells stably expressing mito- $\text{GFP-LAMA}_{\text{F98}}$ , after the wash-out of TMP (50  $\mu\text{M}$ ). Percentage of polylobed cells (mean  $\pm$  s.d. in five independent experiments). Duration of mitotic events recorded in the presence of nocodazole (330 nM) (median  $\pm$  interquartile range,  $N=63$  and 19 cells) and TMP=10  $\mu\text{M}$ , unless otherwise stated. Scale bars, 10  $\mu\text{m}$ . For further details, see statistical analysis.

<sup>GFP</sup>LAMAs can be used to control the localization of other family members of GFP-based proteins to which the enhancer nanobody binds; for example, yellow fluorescent protein and Shadow G<sup>21</sup>, a non-fluorescent version of GFP (Supplementary Fig. 14). The high affinity of <sup>GFP</sup>LAMAs for GFP also allows to mislocalize GFP fusion proteins that are part of larger protein complexes. For example, transient transfection of mito-<sup>GFP</sup>LAMA<sub>F98</sub> into a genome-edited cell line expressing NUP62-monomeric EGFP (mEGFP) (Fig. 2g and Supplementary Fig. 15a), a component of the nuclear pore complex, resulted in sequestration of NUP62-mEGFP from the nuclear envelope to the mitochondria in the absence of TMP (Fig. 2h and Supplementary Fig. 15b). <sup>GFP</sup>LAMA<sub>F98</sub> was expressed as a fusion to SNAP-tag<sup>22</sup>, which allowed its visualization in the transfected cells. On addition of TMP, NUP62-mEGFP localized to the nuclear membrane.

GFP fusion proteins are omnipresent in the life sciences and our <sup>GFP</sup>LAMAs offer a new way to probe the function of these proteins. To demonstrate the potential of <sup>GFP</sup>LAMAs for mechanistic studies, we used mito-<sup>GFP</sup>LAMA<sub>F98</sub> to control the function of a GFP fusion of Mad2L1, an important component of the mitotic checkpoint complex (Fig. 2i and Supplementary Fig. 16). Knock-down of Mad2L1 reduces mitotic duration and increases the percentage of polylobed nuclei<sup>23</sup>. A HeLa Kyoto cell line in which endogenous Mad2L1 has been genome edited and tagged with EGFP has been previously described and used to map the localizations of Mad2L1 during mitosis<sup>24</sup>. We stably expressed mito-<sup>GFP</sup>LAMA<sub>F98</sub> in the Mad2L1-EGFP cell line, and observed how sequestering Mad2L1-EGFP to the mitochondria affected the outcome of cell division (Supplementary Fig. 17 and Supplementary Videos 5–8). We could not generate Mad2L1-EGFP cell lines stably expressing the enhancer nanobody only, presumably because the affinity of the nanobody could not be switched off during the selection process. In the absence of TMP, we observed an increase in the percentage of polylobed nuclei following mitotic events relative to cells not expressing mito-<sup>GFP</sup>LAMA<sub>F98</sub> (85 ± 13% versus 10 ± 6%; Fig. 2j and Supplementary Fig. 18). Addition of TMP to cells expressing mito-<sup>GFP</sup>LAMA<sub>F98</sub> reduced the levels to those not expressing mito-<sup>GFP</sup>LAMA<sub>F98</sub> (10 ± 11%). Next, nocodazole, a small molecule that prevents attachment of microtubules to kinetochores, was added to activate the mitotic checkpoint complex. After treatment with nocodazole, cells in which Mad2L1-EGFP had been sequestered at the mitochondria were able to override mitotic arrest (Fig. 2k), similar to treatment with reversine, a known drug that overrides the mitotic checkpoint<sup>25</sup> (Supplementary Fig. 19). Treatment with nocodazole and TMP lead to mitotic arrest, as expected (Fig. 2k and Supplementary Fig. 19). These data show that the function of Mad2L1-EGFP in the mitotic checkpoint complex can be controlled through its TMP-dependent interaction with mito-<sup>GFP</sup>LAMA<sub>F98</sub>.

In summary, LAMAs are a generally applicable chemogenetic tool to reversibly control the location and function of proteins, including the most commonly used class of fusion proteins (GFP). Nanobodies have been selected for a large variety of targets, all of which could serve as starting point for the generation of new LAMAs. As TMP is a clinically approved drug, the approach might also be applicable in vivo. Furthermore, the design principle introduced here should be applicable for the generation of other switchable proteins.

### Online content

Any methods, additional references, Nature Research reporting summaries, source data, extended data, supplementary information, acknowledgements, peer review information; details of author contributions and competing interests; and statements of data and

code availability are available at <https://doi.org/10.1038/s41592-020-0746-7>.

Received: 17 June 2019; Accepted: 15 January 2020;

Published online: 17 February 2020

### References

1. Hamers-Casterman, C. et al. Naturally occurring antibodies devoid of light chains. *Nature* **363**, 446–448 (1993).
2. Muyldermans, S. Nanobodies: natural single-domain antibodies. *Annu. Rev. Biochem.* **82**, 775–797 (2013).
3. Ingram, J. R., Schmidt, F. I. & Ploegh, H. L. Exploiting nanobodies' singular traits. *Annu. Rev. Immunol.* **36**, 695–715 (2018).
4. Stein, V. & Alexandrov, K. Synthetic protein switches: design principles and applications. *Trends Biotechnol.* **33**, 101–110 (2015).
5. Oakes, B. L. et al. Profiling of engineering hotspots identifies an allosteric CRISPR-Cas9 switch. *Nat. Biotechnol.* **34**, 646–651 (2016).
6. Karginov, A. V., Ding, F., Kota, P., Dokholyan, N. V. & Hahn, K. M. Engineered allosteric activation of kinases in living cells. *Nat. Biotechnol.* **28**, 743 (2010).
7. Gil, A. A. et al. Optogenetic control of protein binding using light-switchable nanobodies. Preprint at *bioRxiv* <https://doi.org/10.1101/739201> (2019).
8. Yu, D. et al. Optogenetic activation of intracellular antibodies for direct modulation of endogenous proteins. *Nat. Methods* **16**, 1095–1100 (2019).
9. Iwakura, M. & Nakamura, T. Effects of the length of a glycine linker connecting the N- and C-termini of a circularly permuted dihydrofolate reductase. *Protein Eng.* **11**, 707–713 (1998).
10. Yu, Q. et al. Semisynthetic sensor proteins enable metabolic assays at the point of care. *Science* **361**, 1122–1126 (2018).
11. Nakamura, T. & Iwakura, M. Circular permutation analysis as a method for distinction of functional elements in the M20 loop of *Escherichia coli* dihydrofolate reductase. *J. Biol. Chem.* **274**, 19041–19047 (1999).
12. Kirchhofer, A. et al. Modulation of protein properties in living cells using nanobodies. *Nat. Struct. Mol. Biol.* **17**, 133–138 (2009).
13. De Genst, E. et al. Molecular basis for the preferential cleft recognition by dromedary heavy-chain antibodies. *Proc. Natl Acad. Sci. USA* **103**, 4586–4591 (2006).
14. Wilton, E. E., Opyr, M. P., Kailasam, S., Kothe, R. F. & Wieden, H.-J. sdAb-DB: the single domain antibody database. *ACS Synth. Biol.* **7**, 2480–2484 (2018).
15. Chaikuad, A. et al. Structure of cyclin G-associated kinase (GAK) trapped in different conformations using nanobodies. *Biochem. J.* **459**, 59–69 (2014).
16. Sosa, B. A. et al. How lamina-associated polypeptide 1 (LAP1) activates torsin. *Elife* **3**, e03239 (2014).
17. Götzke, H. et al. The ALFA-tag is a highly versatile tool for nanobody-based bioscience applications. *Nat. Commun.* **10**, 4403 (2019).
18. Tao, R. et al. Genetically encoded fluorescent sensors reveal dynamic regulation of NADPH metabolism. *Nat. Methods* **14**, 720–728 (2017).
19. Kanaji, S., Iwahashi, J., Kida, Y., Sakaguchi, M. & Mihara, K. Characterization of the signal that directs Tom20 to the mitochondrial outer membrane. *J. Cell Biol.* **151**, 277–288 (2000).
20. Inoue, T., Heo, W. D., Grimley, J. S., Wandless, T. J. & Meyer, T. An inducible translocation strategy to rapidly activate and inhibit small GTPase signaling pathways. *Nat. Methods* **2**, 415–418 (2005).
21. Murakoshi, H., Shibata, A. C. E., Nakahata, Y. & Nabekura, J. A dark green fluorescent protein as an acceptor for measurement of Förster resonance energy transfer. *Sci. Rep.* **5**, 15334 (2015).
22. Keppler, A. et al. A general method for the covalent labeling of fusion proteins with small molecules in vivo. *Nat. Biotechnol.* **21**, 86–89 (2003).
23. Held, M. et al. CellCognition: time-resolved phenotype annotation in high-throughput live cell imaging. *Nat. Methods* **7**, 747–754 (2010).
24. Cai, Y. et al. Experimental and computational framework for a dynamic protein atlas of human cell division. *Nature* **561**, 411–415 (2018).
25. Santaguida, S., Tighe, A., Alise, A. M., Taylor, S. S. & Musacchio, A. Dissecting the role of MPS1 in chromosome biorientation and the spindle checkpoint through the small molecule inhibitor reversine. *J. Cell Biol.* **190**, 73–87 (2010).

**Publisher's note** Springer Nature remains neutral with regard to jurisdictional claims in published maps and institutional affiliations.

© The Author(s), under exclusive licence to Springer Nature America, Inc. 2020

## Methods

**DNA plasmids and molecular cloning.** Plasmids were generated using standard molecular biology techniques. All subcloned sequences were verified using Sanger sequencing, assisted by Geneious software (Biomatters). pCHIV is a noninfectious HIV-1 viral construct lacking long terminal repeats and the *nef* gene<sup>26</sup>. pCHIV env(stop) was described earlier<sup>27</sup> and contains a Klenow Polymerase fill in at the NdeI site to generate a frameshift within the *env* gene. mCherry was inserted between MA (matrix protein) and CA (capsid protein) of the gag polyprotein and was described earlier<sup>28</sup>. pWPI puro was obtained from O. Fackler<sup>29</sup>. psPAX2 was a gift from D. Trono (Addgene plasmid no. 12260) and pCMV-VSV-G was a gift from R. Weinberg (Addgene plasmid no. 8454).

**Chemical reagents.** TMP, pyrimethamine and methotrexate were purchased from Sigma Aldrich. Stock solutions of 50 mM TMP in DMSO were used for both in vitro and in cell analysis. NADPH was purchased from PanReac Biochem, and stocks made to 10 mM fresh in aqueous buffer and used at the indicated concentrations. Nocodazol and reversine were purchased from Selleckchem. DMSO stock solutions were made fresh before use. Fluorescent dyes for live-cell imaging were purchased from available suppliers, or were synthesized as previously described<sup>30,31</sup>.

**Protein purification.** Proteins were expressed using a pET51b(+) (Novagen) in *Escherichia coli* BL21 (DE3) pLysS, in the presence of 100  $\mu\text{g ml}^{-1}$  ampicillin in Luria-Bertani, shaking at 220 r.p.m. Cultures were grown at 37°C until an optical density ( $\text{OD}_{600}$ ) of 0.8 was reached, and then induced with 1 mM isopropyl  $\beta$ -thiogalactopyranoside. After overnight expression at 25°C, cells were collected and lysed by sonication. The lysates were cleared by centrifugation and purified by immobilized metal affinity chromatography (IMAC) using Ni-NTA Resin (Thermo Fisher Scientific). For proteins used in time-resolved-fluorescence resonance energy transfer (TR-FRET) assays, His-tag purification was followed by Strep-Tactin purifications (IBA Lifesciences), according to the manufacturer's protocol.

**Fluorescence emission titrations.** The wtGFP emission assays were performed in 50 mM HEPES, 50 mM NaCl, 0.5  $\text{mg ml}^{-1}$  BSA, 0.05% Triton-X 100 (v/v), pH 7.3, in 384-well plates (Black, flat-bottom, Corning no. 3821). Dilution series of the protein switch in the presence of TMP (500  $\mu\text{M}$ , final concentration) or DMSO and/or NADPH (100  $\mu\text{M}$ , final concentration) were prepared and incubated at room temperature for 10 min. wtGFP (for a 10 nM final concentration in assay) was diluted in 50 mM HEPES, 50 mM NaCl, 0.5  $\text{mg ml}^{-1}$  BSA, 0.05% Triton-X 100, pH 7.3. Protein were then mixed in a 1:1 ratio in the plate, and the plate read in a Spark 20M microplate reader (Tecan). Excitation wavelength was 470 nm (5 nm bandwidth). Emission wavelength was 535 nm (5 nm bandwidth). The titration curves were fitted with the full equation of single site binding, accounting for the effect of nonspecific binding<sup>32</sup>.

**TR-FRET assay.** Constructs assayed by TR-FRET were expressed as SNAP-tag fusions and EGFP-fusions. SNAP-tag on the target proteins (4  $\mu\text{M}$ ) was labeled with an excess of SNAP-Lumi4-Tb (Cisbio) (6  $\mu\text{M}$ ) in 50 mM HEPES, 50 mM NaCl, pH 7.3, at room temperature for 4 h. Excess unlabeled dye was removed by centrifugal filter units (Amicon). Tb-labeled target protein (for a final concentration of 1–20 nM in assays) was diluted in 50 mM HEPES, 50 mM NaCl, 0.5  $\text{mg ml}^{-1}$  BSA, 0.05% Triton-X 100 (v/v), pH 7.3, containing 100  $\mu\text{M}$  NADPH and placed into 384-well plates (Black, flat-bottom, Corning no. 3821). EGFP-fused proteins were diluted in 50 mM HEPES, 50 mM NaCl, 0.5  $\text{mg ml}^{-1}$  BSA, 0.05% Triton-X 100 (v/v), in the presence of TMP (500  $\mu\text{M}$ , final concentration) or DMSO and/or NADPH (100  $\mu\text{M}$ , final concentration). EGFP-fused proteins were mixed in a 1:1 ratio in the plate with the Tb-labeled target and incubated at least 15 min at room temperature. The plate was then read by a Spark 20M microplate reader (Tecan) in TR-FRET mode. The excitation wavelength was 320 nm (25 nm bandwidth). The emission wavelength for Tb was 480 nm (7.5 nm bandwidth), and the emission wavelength for EGFP was 520 nm (7.5 nm bandwidth) using a 510 dichroic mirror. Integration time was 400  $\mu\text{s}$  and lag time 120  $\mu\text{s}$ . The titration curves were fitted to the full equation of single site binding, accounting for the effect of nonspecific binding.

**Kinetics of in vitro dissociation.** wtGFP was mixed with an excess of LAMA (1:3 ratio) on ice for 10 min and passed over size-exclusion chromatography. The heterodimeric fraction was collected and diluted into 50 mM HEPES, 50 mM NaCl, 0.5  $\text{mg ml}^{-1}$  BSA, 0.05% Triton-X 100 (v/v), pH 7.3, in 96-well black flat-bottomed plates to a final concentration of 200 nM, in the presence of 100  $\mu\text{M}$  NADPH. TMP, pyrimethamine or methotrexate were diluted in DMSO to 100 $\times$  the final assay concentration. Then, 1  $\mu\text{l}$  of relevant drug solutions was added to the 96-well plate and fluorescence emission recorded over time on a Spark 20M microplate reader (Tecan). Excitation wavelength was 470 nm (5 nm bandwidth). Emission wavelength was 535 nm (5 nm bandwidth). For reversible association eDHFR was diluted in 50 mM HEPES, 50 mM NaCl, 0.5  $\text{mg ml}^{-1}$  BSA, 0.05% Triton-X 100 (v/v) and 1  $\mu\text{l}$  added to the reaction mix in the 96-well plate. The curves were fitted with one-phase dissociation models to estimate the half time at these concentrations.

**Protein crystallization.** For X-ray crystallography, the LAMAs were subcloned into a vector carrying an N-terminal Hisx10-tag, followed by a tobacco etch virus

(TEV) protease cleavage tag sequence. The production and IMAC purification of the TEV protease was performed as previously described<sup>33</sup>. The His-Tag was removed from the LAMAs by TEV protease cleavage at 30°C overnight, at a ratio of 1:20 (TEV protease: LAMA (w:w)). The digested protein was purified using a reverse IMAC purification method using Ni-NTA resin, collecting the flow-through. The protein was passed over a size-exclusion column and concentrated using centrifugal filter units (Amicon). The protein was flash-frozen and stored at  $-70^\circ\text{C}$  in 25 mM HEPES, 25 mM NaCl, pH 7.3. Purified protein was premixed with NADPH (10 eq) and TMP (10 eq) as solid powders in 300  $\mu\text{l}$  volume. The solution was left on ice for 10 min before centrifugation (20,000g, 10 min, 4°C) to remove any precipitation.

Crystallization was performed at 20°C using the vapor-diffusion method. Crystals of <sup>6FP</sup>LAMA<sub>F98</sub>:NADPH:TMP complex with a rod morphology were grown by mixing equal volumes of protein solution at 25  $\text{mg ml}^{-1}$  in 25 mM HEPES, 25 mM sodium chloride pH 7.3 and a reservoir solution containing 0.1 M MES pH 6.0, 30% (v/v) PEG 600, 5% (w/v) PEG 1000 and 10% (v/v) glycerol. The crystals were briefly washed in cryoprotectant solution consisting of the reservoir solution with sucrose and glucose added to a final concentration of 10% (w/v) each, before flash-cooling in liquid nitrogen. <sup>6FP</sup>LAMA<sub>G97</sub>:NADPH:TMP complex crystals were obtained by mixing equal volumes of protein solution at 15  $\text{mg ml}^{-1}$  in 25 mM HEPES, 25 mM sodium chloride pH 7.3 and precipitant solution containing 0.1 M MES pH 6.0, 20% (w/v) PEG 6000 and 1.0 M lithium chloride. Thin plate-shaped crystals grew in clusters; single plates could be isolated and were briefly washed in cryoprotectant solution consisting of the reservoir solution supplemented with 20% (v/v) glycerol before flash-cooling in liquid nitrogen.

**X-ray diffraction data collection and structure determination.** Single crystal X-ray diffraction data were collected at 100 K on the X10SA beamline at the SLS (PSI). All data were processed with XDS<sup>34</sup>. The structures were determined by molecular replacement using Phaser<sup>35</sup> and individual protein coordinates from PDB entries 5UII and 5H8D as search models for DHFR and nanobody, respectively. The final models were optimized in iterative cycles of manual rebuilding using Coot<sup>36</sup>, and refinement using Refmac5 (ref. <sup>37</sup>) and phenix.refine<sup>38</sup>. Data collection and refinement statistics are summarized in Supplementary Table 1, model quality was validated with MolProbity<sup>39</sup> as implemented in PHENIX. The omit maps for ligands were generated using the composite omit map tool in PHENIX<sup>38</sup>.

Atomic coordinates and structure factors have been deposited in the Protein Data Bank (PDB) under accession codes 6RUL (<sup>6FP</sup>LAMA<sub>F98</sub>) and 6RUM (<sup>6FP</sup>LAMA<sub>G97</sub>). Analysis was conducted using MacPyMOL<sup>40</sup> and Coot<sup>36</sup>.

**Mammalian cell culture maintenance.** Eukaryotic cells were obtained from American Type Culture Collection (ATCC), The Leibniz Institute DSMZ-German Collection of Microorganisms and Cell Cultures, or from collaborators as indicated. No cell lines on the ICLAC list of commonly misidentified cells were used in this work. All cells were cultured in DMEM GlutaMax (Thermo Fisher Scientific) medium supplemented with 10% FBS, and penicillin and streptomycin as indicated, at 37°C in a humidified incubator with 5% CO<sub>2</sub>. All cells were mycoplasma free.

**Generation of <sup>P24</sup>LAMA<sub>98</sub> cell lines.** Lentiviral particles were generated by cotransfection of transfer plasmid pWPI EGFP-<sup>P24</sup>LAMA<sub>98</sub> IRES puro, packaging construct psPAX2, envelope protein expression plasmid pCMV-VSVG and pAdvantage (Promega) in a ratio of 1.5: 1: 0.5: 0.2, into HEK293T (ATCC) cells using PEI (1:3 ratio of  $\mu\text{g DNA}$ :  $\mu\text{l 1 mg ml}^{-1}$  PEI). The medium was changed after 6 h and production of lentiviral particles was allowed to proceed for 48 h. The supernatant was filtered through 0.45  $\mu\text{m}$  MCE filters and was directly added to HeLa TZM-bl cells (NIH AIDS Repository). After 2 d the cells were expanded and 1  $\mu\text{g ml}^{-1}$  puromycin was added to select for stably transduced cells.

**Genome editing.** Nup62 in HeLa Kyoto cells was endogenously tagged with mEGFP at the C terminus by CRISPR-Cas9 nickases and its homozygous integration was validated as described previously<sup>41,42</sup>. The guide RNA sequences for the genome editing are as follows: 5'TCGCTCAGTCAAAGGTGATC3' and 5'CTGGGGCCCCGAGGTCCCTA3'.

Previously described genome-edited HeLa Kyoto Mad2L1-EGFP<sup>24</sup> were used in the generation of stable cell lines expressing LAMAs. HeLa Kyoto Mad2L1-EGFP cells were seeded 1 d before transfection with pcDNA3.0 vectors with Lipofectamin3000 (Thermo Fisher Scientific), in the presence of TMP (10–50  $\mu\text{M}$ ), following the manufacturer's instructions. Cells were seeded monoclonal densities and selected using 500–800  $\mu\text{g ml}^{-1}$  geneticin (Thermo Fisher Scientific) and TMP (10–50  $\mu\text{M}$ ) for 2 weeks. Cells were then labeled with BG-SiR (500 nM) overnight, before sorting on a FACSMelody (BD biosciences) for LAMA expressing cells.

**Live-cell imaging of LAMA in CHIV (replication-defective HIV-1) expressing cells.** HeLa TZM-bl cells were seeded in eight-well Lab-Tek (nunc) at 20,000 cells per well the day before transfection in complete medium with 100 U  $\text{ml}^{-1}$  penicillin 100  $\mu\text{g ml}^{-1}$  streptomycin and incubated at 37°C and 5% CO<sub>2</sub>. pCHIV env(stop) was transfected in a 1:1 ratio with pCHIV env(stop) gag-mCherry

using Turbofect (1:2 ratio). The cells were incubated for 24 h, the medium was changed to imaging medium (FluoroBrite DMEM (Thermo Fisher Scientific), 10% FBS, 4 mM GlutaMAX (Gibco Life Technologies), 2 mM sodium pyruvate (Gibco Life Technologies), 20 mM HEPES pH 7.4, 100 U ml<sup>-1</sup> penicillin 100 µg ml<sup>-1</sup> streptomycin (PAN-Biotech)) and transferred to a Nikon Eclipse Ti2 (Nikon, Japan) inverted microscope equipped with an Andor confocal spinning disk unit (Yokogawa CSU-W1 Spinning Disk Unit, Andor, Oxford Instruments). Cells were imaged at 37 °C and 5% CO<sub>2</sub> using a ×100 oil-immersion objective (Nikon CFI Apochromat TIRF ×100 Oil, numerical aperture (NA) 1.49) and a dual electron-multiplying charge-coupled device camera setup (Andor iXon DU-888), simultaneously recording the EGFP (488/500–550 nm) and the mCherry channel (568/575–625 nm) with a pixel size of 0.13 µm. Three-dimensional stacks (0.5 µm, z-spacing) were recorded with a time interval of 3 min for 60–120 min at up to 32 randomly chosen positions using the Nikon Imaging Software Elements 5.02. After 4–12 frames, 50 µl of TMP containing imaging medium was added to a final concentration of 10 µM and imaging was continued. For presentation purposes, the movies were filtered in FIJI/ImageJ<sup>43</sup> with a mean filter (kernel size, 0.25 × 0.25 µm) to reduce noise. For quantification of the raw data, the mean intensity of a region of interest (ROI) inside the nucleus was measured using the Multi Measure function of the ROI Manager. Camera background was subtracted and intensities were normalized to the highest intensity within the ROI during the timeseries to correct for different expression levels. Different experiments were temporally aligned to the time of TMP addition and data was pooled from three independent experiments.

**Perfusion of TMP over live cells.** HeLa Kyoto cells<sup>41</sup> were transfected with Lipofectamin2000 (Thermo Fisher Scientific) according to the manufacturer's protocol. After 24 h, cells were seeded on Ibidi 0.6 Luer I cell culture treated perfusion chambers at 24,000 cells per chamber. All perfusion experiments were performed in complete DMEM GlutMax medium without phenol red. After the cells were adherent, BG-SiR (500 nM) was added to the perfusion chamber and labeled overnight at 37 °C. The perfusion chamber was then attached to a syringe pump, with a 20 ml syringe, and mounted on a Leica DMi8 microscope (Leica Microsystems) equipped with a Leica TCS SP8 X scanhead, a SuperK white-light laser and an HC PL APO ×40/1.10 W motCORR CS2 objective, at 37 °C. TMP (10 µM) was perfused over the cells at a flow rate of 1.5 ml min<sup>-1</sup>, and images acquired at a scanning speed of 400 Hz, pixel dwell time 600 ns, pixel size 0.09 µm, with a pinhole at 1 airy unit, with z-stacks of 2 over 12 µm, with image acquisition every 18.24 s. A white-light laser was used for excitation, collecting with Leica HyD detectors: EGFP (488/505–550 nm), SiR (633/650–750 nm). Image analysis was conducted in FIJI/ImageJ using the Time Series Analyzer (3.0), selecting an ROI in the nucleus and measuring the fluorescent intensity over time, with background subtraction of a region outside the cells. All values were normalized to the intensity in the nucleus 13 min after TMP perfusion. Different experiments were temporally aligned to the time of TMP addition and data was pooled from three independent experiments.

**Live-cell imaging of Nup62-mEGFP.** Live-cell imaging of HeLa Nup62-mEGFP cells was performed at 37 °C in CO<sub>2</sub>-independent medium without phenol red (Invitrogen) containing 20% FBS, 2 mM l-glutamine and 100 µg ml<sup>-1</sup> penicillin and streptomycin, with either 10 µM of TMP or DMSO (0.1% (v/v)). Cells were seeded on eight-well Lab-Tek Chambered Coverglass (Thermo Fisher Scientific) at 10,000 cells per well. Cells were incubated with 10 µM BG-TMR for 30 min and the BG-TMR was washed away before imaging. Cells were then observed by confocal microscopy (LSM780, Carl Zeiss) using a ×63, 1.4 NA Plan-Apochromat objective (Carl Zeiss), recording the mEGFP (488/491–552 nm) and TMR (561/580–660 nm) channels with a xy resolution of 0.13 µm and the section thickness of 1.2 µm. Fluorescence images were filtered with a median filter (kernel size, 0.25 × 0.25 µm<sup>2</sup>) for presentation purposes.

**Automated microscopy and analysis.** For continuous live-cell imaging of HeLa Kyoto Mad2L1-EGFP cells stably expressing LAMAs, cells were seeded in 96-well plates (Eppendorf), in the presence of TMP (50 µM) at 10,000 cells per well. After cells were adherent, SNAP-tag in the fusion proteins was labeled with BG-SiR (100 nM) overnight. The cells were then labeled with Hoechst 33342 (1 µg ml<sup>-1</sup>) in complete medium without phenol red in the presence or absence of TMP (50 µM) for 15 min, and washed three times with complete medium without phenol red in the presence or absence of TMP (50 µM). Cells were imaged in the presence of BG-SiR (100 nM), in the presence or absence of TMP (50 µM), and in the presence of additional mitotic drugs as indicated, nocodazole (330 nM) or reversine (5 µM). Automatic microscopy was conducted using Leica HCS A Matrix Screener software on a Leica DMi8 microscope (Leica Microsystems) equipped with a Leica TCS SP8 X scanhead, a SuperK white-light laser and an HC PL APO ×40/1.10 W motCORR CS2 objective, at 37 °C, 5% CO<sub>2</sub>, achieved by a temperature controllable incubator (Life Imaging Services). A white-light laser or 405 nm diode was used to excite the fluorophores, collecting with Leica HyD detectors: Hoechst (405/425–475 nm), SiR (633/650–750 nm). Image acquisition was conducted at a speed of 400 Hz, pixel dwell time 1.2 µs, pixel size 0.57 µm, with z-stacks of 1 over 10 µm. Image analysis was conducted in FIJI/ImageJ, with manual annotations of LAMA expressing cells followed from prometaphase to mitotic exit.

**Fitting models for in vitro characterization.** The full equation for single site binding, accounting for the effect of nonspecific binding was used to fit the wtGFP fluorescence emission assay and TR-FRET assay:

$$y = (F_{\max} - F_{\min}) \times F_{\text{sb}} + F_{\max} + N \times x$$

where

$$F_{\text{sb}} = \frac{(L + x + K_d - \sqrt{(L + x + K_d)^2 - 4 \times L \times x})}{2 \times L}$$

where  $y$  is the emission at 535 nm,  $F_{\text{sb}}$  is the fraction of protein bound,  $F_{\max}$  and  $F_{\min}$  are the maximum and minimum emission values,  $x$  is the concentration of nanobody protein titrated into wtGFP or the Tb-labeled target,  $N$  is a parameter for nonspecific binding,  $L$  is the total concentration of wtGFP or Tb-labeled target ( $L = 1\text{--}20$  nM) and  $K_d$  is the calculated dissociation constant between the nanobody derivative and wtGFP or Tb-labeled target.

**One-phase association and dissociation for kinetic measurements in vitro and in cellulo.** Time-series data of association were fit with a pseudo first-order exponential model, according to:

$$y = NS + (y_0 - NS) \times (1 - e^{-kt})$$

$$t_{1/2} = \frac{\ln(2)}{k}$$

where  $y$  is the measured intensity,  $y_0$  is the intensity at time 0,  $NS$  is the minimal intensity measured at infinite time,  $k$  is the pseudo-first-order rate constant,  $t$  is the time and  $t_{1/2}$  is the half time.

Time-series data of dissociation were fit with a pseudo first-order exponential model, according to:

$$y = y_0 + (y_{\max} - y_0) \times (1 - e^{-kt})$$

where  $y$  is the measured intensity,  $y_0$  is the intensity at time 0,  $y_{\max}$  is the maximal intensity measured,  $k$  is the pseudo-first-order rate constant and  $t$  is the time.

**ITC.** Proteins were dialyzed using mini dialysis kits (GE Healthcare) containing NADPH (1 mM) and/or TMP (0.5 mM of DMSO) as indicated. The protein concentrations were measured by A<sub>280</sub> using a nanodrop (1 mm pathlength). The molar extinction coefficient was estimated using the Geneious software (Biomatters). A Microcal PEAQ-ITC microcalorimeter was used for the measurements. Protein concentration ranged from 10 to 40 µM in the cell, and a 10-fold excess in the syringe. Eight- or 13-injection programs were chosen depending on the expected affinity between the molecular entities.

**Translocation of fluorescent proteins.** HeLa Kyoto cells were seeded in 96-well plates (Eppendorf) at 10,000 cells per well 24 h before transfection with Lipofectamin2000 (Thermo Fisher Scientific) according to the manufacturer's protocol. After 24 h, complete medium without phenol red was added to the cells. Cells were labeled with BG-SiR (500 nM) overnight, in the presence or absence of 10 µM TMP or DMSO (0.1% v/v), before being imaged by confocal microscopy using a Leica DMi8 microscope (Leica Microsystems) equipped with a Leica TCS SP8 X scanhead; a SuperK white-light laser, and an HC PL APO ×40/1.10 W motCORR CS2 objective, at 37 °C with 5% CO<sub>2</sub>, achieved by a temperature controllable incubator (Life Imaging Services). Image acquisition was conducted at a speed of 400 Hz, pixel dwell time of 600 ns, pixel size 0.06 µm, with z-stacks of 1 over 10 µm. A white-light laser was used for excitation, collecting with Leica HyD detectors: EGFP (488/505–550 nm), yellow fluorescent protein (514/525–573 nm), ShadowG-mScarlet (561/583–625 nm) and SiR (633/650–750 nm).

**Genome-edited NUP62-EGFP.** The probe sequences for Southern blotting are as follows.

Nup62-mEGFP: 5' AACCTAGTGGCACCAGAGTAACCTAGTCAGTTACAGTAAAAATCCACTGTGTGTGGAAGGCAGAACTAGCGGTTGTATCCCAAGCATCTTTTGTATTGTCTTTATACTTTGCTGTAATCTCTGAAATACCT-ATTACTGTATGTTGCTTTTCTAAATAAATGATTGTGAAACCAAAACAGCTGCTGTTAATATGGATAAATGTTAGGAGGAGAAAGCTGAGTAAAAAGAGCCAGGTCCAGGAGACTCTGCAGGGGTGCCATTACATGAAACGCACAGGCAAGCAAAATGAAGTAGTGTTCATATAGACATAGGGGTATCGATGAAGCAGCTTTTGTGTTGATGAGACAGAGTAATAGACAAAATGCAAATCGTGGTTT GCTCCAGGAA3';

mEGFP: 5' CACATGAAGCAGCAGACTTCTTCAAGTCCGCCATGCCCGAAGGCTACGTCAGGAGCGCACCATCTTCTTCAAGGACGCGCAAC-TACAAGACCGCGCCGAGGTGAAGTTCGAGGCGCACCTGGTGAACCGCATCGAGCTGAAGGGCATCGACTCAAGGAGGACGCGCAACATCCTGGGCAACAAGCTGAGTACAACACTACAACGCCAACGCTCTATATCATATGGCCGACAAGCAGAAGAACGGCATCAAGGTGAACCTCAAGATCCGCCACAAC

ATCGAGGACGGCAGCGTGCAGCTCGCCGACCTACCAGCAGA ACACCC3'.

**Statistical analysis.** The titrations in Fig. 1c–e,j,l were performed in triplicates in at least three independent experiments with similar results. The in vitro kinetics was measured in triplicates in three independent experiments with similar results. The mean  $\pm$  s.d. is plotted for these experiments.

For live-cell imaging of LAMAs in Fig. 2b,d, representative images are shown from three independent experiments with similar results. For analyzing the kinetics of GFP-LAMAs in live cells in Fig. 2e,f, data was plotted as the mean  $\pm$  s.e.m. from three independent perfusions with  $N=14$  cells for GFP-LAMA<sub>F98</sub> and  $N=9$  cells for GFP-LAMA<sub>G97</sub>. In Fig. 2h, experiments were performed twice independently and the sequestering was reliably reproduced. For scoring nuclear morphology after mitosis in Fig. 2j, five time-lapse series from independent experiments were manually scored and the percentage of polylobed cells is plotted as the mean  $\pm$  s.d. For scoring the time spent in mitosis in Fig. 2k, data from three independent time-lapse series were manually scored and plotted as the median  $\pm$  interquartile range. The total number of cells analyzed that underwent mitosis during time-lapse imaging was  $N=63$  for wash-out of TMP with DMSO and  $N=19$  for cells kept in TMP.

For details of statistical analysis in the Supplementary Figures, see respective figure legends.

**Reporting Summary.** Further information on research design is available in the Nature Research Reporting Summary linked to this article.

### Data availability

Plasmids encoding for LAMAs have been deposited on Addgene with accession codes 130704 to 130718 and 136618 to 136635. All requests for the Nup62-mEGFP genome-edited cell line should be directed to J.E. Structures of GFP-LAMA<sub>F98</sub> and GFP-LAMA<sub>G97</sub> have been deposited to the PDB with deposition codes 6RUL and 6RUM, respectively. The source data for Figs. 1c–g,j,l and 2e,f,j,k are provided with the paper online. Additional datasets that support the finding of this study are available from the corresponding author upon request.

### References

- Müller, B. et al. Construction and characterization of a fluorescently labeled infectious human immunodeficiency virus type 1 derivative. *J. Virol.* **78**, 10803–10813 (2004).
- Lampe, M. et al. Double-labelled HIV-1 particles for study of virus–cell interaction. *Virology* **360**, 92–104 (2007).
- Hendrix, J. et al. Live-cell observation of cytosolic HIV-1 assembly onset reveals RNA-interacting Gag oligomers. *J. Cell Biol.* **210**, 629–646 (2015).
- Trotard, M. et al. Sensing of HIV-1 infection in Tzm-bl cells with reconstituted expression of STING. *J. Virol.* **90**, 2064–2076 (2016).
- Lukinavičius, G. et al. A near-infrared fluorophore for live-cell super-resolution microscopy of cellular proteins. *Nat. Chem.* **5**, 132–139 (2013).
- Keppler, A., Pick, H., Arrivoli, C., Vogel, H. & Johnsson, K. Labeling of fusion proteins with synthetic fluorophores in live cells. *Proc. Natl Acad. Sci. USA* **101**, 9955–9959 (2004).
- Roehrl, M. H. A., Wang, J. Y. & Wagner, G. A general framework for development and data analysis of competitive high-throughput screens for small-molecule inhibitors of protein–protein interactions by fluorescence polarization. *Biochemistry* **43**, 16056–16066 (2004).
- Cabrita, L. D. et al. Enhancing the stability and solubility of TEV protease using in silico design. *Protein Sci.* **16**, 2360–2367 (2009).
- Kabsch, W. XDS. *Acta Crystallogr. D. Struct. Biol.* **66**, 125–132 (2010).
- McCoy, A. J. et al. Phaser crystallographic software. *J. Appl. Crystallogr.* **40**, 658–674 (2007).
- Emsley, P., Lohkamp, B., Scott, W. G. & Cowtan, K. Features and development of Coot. *Acta Crystallogr. D. Biol. Crystallogr.* **66**, 486–501 (2010).
- Murshudov, G. N. et al. REFMAC5 for the refinement of macromolecular crystal structures. *Acta Crystallogr. D. Struct. Biol.* **67**, 355–367 (2011).
- Adams, P. D. et al. PHENIX: a comprehensive Python-based system for macromolecular structure solution. *Acta Crystallogr. D. Biol. Crystallogr.* **66**, 213–221 (2010).
- Chen, V. B. et al. MolProbity: all-atom structure validation for macromolecular crystallography. *Acta Crystallogr. D. Biol. Crystallogr.* **66**, 12–21 (2010).
- DeLano, W. L. Pymol: an open-source molecular graphics tool. CCP4 newsletter on protein. *Crystallography* **40**, 82–92 (2002).
- Koch, B. et al. Generation and validation of homozygous fluorescent knock-in cells using CRISPR–Cas9 genome editing. *Nat. Protoc.* **13**, 1465–1487 (2018).
- Otsuka, S. et al. Postmitotic nuclear pore assembly proceeds by radial dilation of small membrane openings. *Nat. Struct. Mol. Biol.* **25**, 21–28 (2018).
- Schindelin, J. et al. Fiji: an open-source platform for biological-image analysis. *Nat. Methods* **9**, 676–682 (2012).

### Acknowledgements

This work was supported by the Max Planck Society, the École Polytechnique Fédérale de Lausanne and NCCR Chemical Biology. Research in Kräusslich's group was supported by the Deutsche Forschungsgemeinschaft (DFG, German Research Foundation) (Projektnummer 240245660) SFB 1129 project 5 (H.-G.K.). Research in Ellenberg's group was supported by the Paul G. Allen Frontiers Group through an Allen Distinguished Investigators Grant to J.E., the National Institutes of Health Common Fund 4D Nucleome Program (grant no. U01 EB021223/U01 DA047728 to J.E.) and the EMBL (S.O., M.K. and J.E.). We thank I. Schlichting for X-ray data collection. Diffraction data were collected at the Swiss Light Source, beamline X10SA, of the Paul Scherrer Institute, Villigen, Switzerland. We thank L. Reymond, J. Broichhagen, B. Mathes and A. Bergner for providing reagents and M. Eguren for valuable discussions.

### Author contributions

H.F. and K.J. designed the study. H.F. generated, characterized and applied all LAMAs. M.T. solved the crystal structures of GFP-LAMAs. J.H. helped analyze the crystal structures. M.K. generated the NUP62-mEGFP cell line and S.O. performed the NUP62-mEGFP translocation experiments. B.K. helped with generation of stable cell lines with LAMAs. T.G.M. generated stable cell lines of P<sup>24</sup>LAMA and characterized them. H.-G.K., J.E. and K.J. supervised the work. H.F. and K.J. wrote the manuscript with input from all authors.

### Competing interests

The authors declare no competing interests.

### Additional information

**Supplementary information** is available for this paper at <https://doi.org/10.1038/s41592-020-0746-7>.

**Correspondence and requests for materials** should be addressed to K.J.

**Peer review information** Arunima Singh was the primary editor on this article and managed its editorial process and peer review in collaboration with the rest of the editorial team.

**Reprints and permissions information** is available at [www.nature.com/reprints](http://www.nature.com/reprints).

## Reporting Summary

Nature Research wishes to improve the reproducibility of the work that we publish. This form provides structure for consistency and transparency in reporting. For further information on Nature Research policies, see [Authors & Referees](#) and the [Editorial Policy Checklist](#).

### Statistics

For all statistical analyses, confirm that the following items are present in the figure legend, table legend, main text, or Methods section.

n/a Confirmed

- The exact sample size ( $n$ ) for each experimental group/condition, given as a discrete number and unit of measurement
- A statement on whether measurements were taken from distinct samples or whether the same sample was measured repeatedly
- The statistical test(s) used AND whether they are one- or two-sided  
*Only common tests should be described solely by name; describe more complex techniques in the Methods section.*
- A description of all covariates tested
- A description of any assumptions or corrections, such as tests of normality and adjustment for multiple comparisons
- A full description of the statistical parameters including central tendency (e.g. means) or other basic estimates (e.g. regression coefficient) AND variation (e.g. standard deviation) or associated estimates of uncertainty (e.g. confidence intervals)
- For null hypothesis testing, the test statistic (e.g.  $F$ ,  $t$ ,  $r$ ) with confidence intervals, effect sizes, degrees of freedom and  $P$  value noted  
*Give  $P$  values as exact values whenever suitable.*
- For Bayesian analysis, information on the choice of priors and Markov chain Monte Carlo settings
- For hierarchical and complex designs, identification of the appropriate level for tests and full reporting of outcomes
- Estimates of effect sizes (e.g. Cohen's  $d$ , Pearson's  $r$ ), indicating how they were calculated

*Our web collection on [statistics for biologists](#) contains articles on many of the points above.*

### Software and code

Policy information about [availability of computer code](#)

Data collection

Plate reader: Tecan Sparkcontrol Method Editor V.2.2  
Microscopy: Leica LAS X 3.1.1.15751 with HCSA Multiwell Full SP8 MAtRix Screener Software Module (No. 156602533, 2017), ZEN software 2012 SP1 (8.1.0.484) and Nikon Imaging Software Elements 5.02.  
ITC: MicroCal PEAQ-ITC (MAL1177030)  
Åkta Pure: using Unicorn 7.1 Build (7.1.0.378)

Data analysis

Microsoft Excel for Mac (version 16.16.16(191111)), Fiji/ImageJ (version 2.9.9-rc-69/1.52p, build: 269a0ad53f), Graphpad Prism (version 8.0.2), MicroCal PEAQ-ITC Analysis software (version 1.1.0.126), XDS (version Jan 26, 2018 BUILT=20180126), Refmac5 (versions 5.8.0222 and 5.8.0232), Phaser (version 2.8.2), PHENIX (version 1.14rc1-3177), MacPyMol (v1.8.4.0) and Coot (version 0.8.9.1).

For manuscripts utilizing custom algorithms or software that are central to the research but not yet described in published literature, software must be made available to editors/reviewers. We strongly encourage code deposition in a community repository (e.g. GitHub). See the Nature Research [guidelines for submitting code & software](#) for further information.

### Data

Policy information about [availability of data](#)

All manuscripts must include a [data availability statement](#). This statement should provide the following information, where applicable:

- Accession codes, unique identifiers, or web links for publicly available datasets
- A list of figures that have associated raw data
- A description of any restrictions on data availability

There are no restrictions on data availability.

## Field-specific reporting

Please select the one below that is the best fit for your research. If you are not sure, read the appropriate sections before making your selection.

Life sciences       Behavioural & social sciences       Ecological, evolutionary & environmental sciences

For a reference copy of the document with all sections, see [nature.com/documents/nr-reporting-summary-flat.pdf](https://www.nature.com/documents/nr-reporting-summary-flat.pdf)

## Life sciences study design

All studies must disclose on these points even when the disclosure is negative.

Sample size	Sample size was based on experience in prior studies, for example Cai et al 2018 (Nature). All Mad2L1-EGFP/GFP-LAMA experiments were performed at least in three different cell cultures, which gave enough observations of mitosis for cell cycle analysis.
Data exclusions	For continuous live cell imaging of mitosis, the pre-established exclusion criteria were as follows: cells which did not express the protein of interest were excluded from the analysis (no SiR signal from labeling SNAP-tag). Cells which did not have a clear fate after mitosis and cells that underwent cell death during the time course were not included in the analysis. For perfusion experiments of GFP-LAMAs, the pre-established exclusion criteria was: data from cells out-of-focus during perfusion were not included in the analysis. No other data was excluded.
Replication	Screening of insertion positions were performed once in duplicates. All validation and further experiments of LAMAs were performed in minimum triplicates, on multiple cell culture replicates, and in multiple experiments. All replicates were successful.
Randomization	No randomization was applied, due to the nature of the experiments.
Blinding	No blinding of experimental set ups or analysis were applied, due to the nature of the experiments.

## Reporting for specific materials, systems and methods

We require information from authors about some types of materials, experimental systems and methods used in many studies. Here, indicate whether each material, system or method listed is relevant to your study. If you are not sure if a list item applies to your research, read the appropriate section before selecting a response.

### Materials & experimental systems

### Methods

n/a	Involved in the study
<input checked="" type="checkbox"/>	<input type="checkbox"/> Antibodies
<input type="checkbox"/>	<input checked="" type="checkbox"/> Eukaryotic cell lines
<input checked="" type="checkbox"/>	<input type="checkbox"/> Palaeontology
<input checked="" type="checkbox"/>	<input type="checkbox"/> Animals and other organisms
<input checked="" type="checkbox"/>	<input type="checkbox"/> Human research participants
<input checked="" type="checkbox"/>	<input type="checkbox"/> Clinical data

n/a	Involved in the study
<input checked="" type="checkbox"/>	<input type="checkbox"/> ChIP-seq
<input checked="" type="checkbox"/>	<input type="checkbox"/> Flow cytometry
<input checked="" type="checkbox"/>	<input type="checkbox"/> MRI-based neuroimaging

## Eukaryotic cell lines

Policy information about [cell lines](#)

Cell line source(s)	HEK293 (CRL-3216; RRID: CVCL_0063) provided by ATCC. HeLa TZM-bl (Cat# 8129; RRID: CVCL_B478) provided by NIH AIDS Repository. Wildtype HeLa Kyoto cells (RRID: CVCL_1922; kind gift from Prof. Narumiya in Kyoto University).
Authentication	Cell lines were not further authenticated.
Mycoplasma contamination	Cell lines have been tested and are negative.
Commonly misidentified lines (See <a href="#">ICLAC</a> register)	No commonly misidentified cell lines were used.